Title
Estimation of River Depth from Remotely Sensed Hydraulic Relationships

Author
Mersel, Matthew King

Publication Date
2012

Peer reviewed|Thesis/dissertation

UNIVERSITY OF CALIFORNIA

Los Angeles

Estimation of River Depth from Remotely Sensed Hydraulic Relationships

A thesis submitted in partial satisfaction

of the requirements for the degree Master of Arts

in Geography

by

Matthew King Mersel

2012

ABSTRACT OF THE THESIS

Estimation of River Depth from Remotely Sensed Hydraulic Relationships

by

Matthew King Mersel

Master of Arts in Geography

University of California, Los Angeles, 2012

Professor Laurence Smith, Chair

The Surface Water and Ocean Topography (SWOT) radar interferometer satellite mission will provide unprecedented global measurements of water surface elevation (*WSE*) for inland water bodies. However, like most remote-sensing technologies SWOT will not observe river channel bathymetry below the water surface, thus limiting its value for estimating river discharge. This study explores the possibility of using remotely sensed observations of river flow width and *WSE* alone to estimate this unmeasured flow depth. Synthetic values of *WSE* and either cross-sectional flow width (w) or effective width (W_e, inundated area divided by reach length) are extracted from 1,495 surveyed channel cross-sections and 62 km of continuously acquired sonar data for the Upper Mississippi, Illinois, Rio Grande, and Ganges-Brahmaputra river systems. A method is presented which uses extrapolation of low-flow width-*WSE* relationships to estimate d, at locations where two distinct hydraulic relationships, one for moderate-to-high flows and one for low-flows, are identified (called the "Slope-break Method,"

owing to detection of two clearly different linear trends in width-*WSE* relationships at these locations). These slope-break relationships represent a subset of "optimal" locations where river flow width and *WSE* co-vary with relative predictably. Slope-breaks were discovered in all four river systems at 6 (.04%) to 242 (16%) of the 1,495 studied cross-sections for channel bathymetric exposures ranging from 20% to 95%, respectively. Depth estimates generated by the Slope-break Method produced root mean squared errors (RMSE) of less than 20% (relative to bankfull mean depth) for the Upper Mississippi, Illinois, Rio Grande, and Ganges-Brahmaputra river systems when channel exposure was >25%, >50%, >75%, and >75%, respectively. HEC-RAS modeling for the Upper Mississippi and Rio Grande rivers suggests that these channel exposures occur at least ~25% and ~42% of the time, respectively, based on historic discharge records and steady-state discharge simulations. "Reach-averaging" (spatial averaging) of retrieved hydraulic variables reduces both RMSE and longitudinal variability in the derived depth estimates, especially at reach lengths of ~1000-2000 m. The findings presented here have positive implications for SWOT and other sensors attempting to estimate river flow depth and/or discharge solely from incomplete, remotely sensed hydraulic variables, and suggest that useful depth retrievals can be obtained even given the spatial and temporal constraints of spaceborne observations.

The thesis of Matthew King Mersel is approved.

Gregory Stewart Okin

Yongwei Sheng

Laurence Smith, Committee Chair

University of California, Los Angeles

2012

This thesis is dedicated to my mother, Cinda, who has given me a lifetime of love, support, and guidance.

Table of Contents

List of Figures

Acknowledgements

A special thank you goes to Laurence C. Smith, my graduate advisor and committee chair who has provided me with invaluable knowledge and guidance over the past two years, and without whom none of this work would have been possible. Many thanks go to Konstantinos Andreadis and Michael Durand for their contribution and support, and who helped guide the direction of this work, as well as to my committee members, Yongwei Sheng and Greg Okin for their feedback. I also owe my gratitude to Scott Stephenson, Vena Chu, Colin Gleason, and Jida Wang, for the help and input they have provided over the past two years and to the many other people in the Department of Geography at UCLA who have helped me along the way. I am extremely grateful to my family – my mother, father, and grandmother, Gammy – who have provided me with endless love and support. I gratefully acknowledge Edward Beighley and Faisal Hossain, as well as the U.S. Army Corps of Engineers, USGS, Institute of Water Modeling (IWM) – Bangladesh, and Tetra Tech. Inc. for the datasets used in this study. Funding for this work was provided by the NASA Physical Oceanography Program (grant #NNX10AE96G), managed by Eric Lindstrom, and by the Graduate Division at UCLA. The PI on this grant is Michael Durand (Department of Geological Sciences, The Ohio State University), and the Co-PIs are Laurence C. Smith (Department of Geography, UCLA) and Konstantinos Andreadis (Jet Propulsion Laboratory). This work is in preparation for submission to be published in an academic journal (co-authors are Laurence C. Smith, Konstantinos Andreadis, and Michael Durand).

1. Introduction

Terrestrial runoff to rivers is a significant term in the global water balance and a principle source of fresh water for human and ecosystem use [*Vorosmarty et al.*, 2010], yet global knowledge of the spatial and temporal dynamics of river flow is surprisingly poor [*Alsdorf et al.*, 2007b; *Durand et al.*, 2010a]. Stream gages, the traditional method for measuring discharge, are in decline globally [*Stokstad*, 1999; *Shiklomanov et al.*, 2002], and where gages do exist, the data are often unreliable or not publically released [*Alsdorf et al.*, 2007b]. Furthermore, gages are inherently limited to providing information only at single points along a river and fail to capture three-dimensional dynamics of fluvial systems including overbank flow, flood waves, and multichannel flow. These limitations, combined with rising worldwide stress on river systems owing to industrialization, population growth, and climate change [*World Water Assessment Programme*, 2012] motivate development of new approaches for understanding river dynamics globally.

Remote sensing of rivers is a relatively immature but rapidly emerging subdiscipline within hydrology that is advancing new approaches to studying fluvial systems [*Smith*, 1997; *Alsdorf et al.*, 2007b; *Durand et al.*, 2010a; *Marcus and Fonstad*, 2010]. Furthermore, the unique spatial perspective afforded from satellites and aircraft allows for observation and understanding of rivers in ways both infeasible and fundamentally different from traditional ground-based methods. One approach is the use of profiling oceanographic radar altimeters to retrieve point measurements of water surface elevation (*WSE*) where orbit paths cross water bodies [e.g. *Koblinsky et al.*, 1993; *Birkett*, 1998; *Birkett et al.*, 2002; *Frappart et al.*, 2005; *Cretaux and Birkett*, 2006; *Calmant et al.*, 2008; *Birkett and Beckley*, 2010; *Lee et al.*, 2011]. However, such techniques are generally limited to large rivers, lakes and reservoirs and, like stream gages, are

inherently point-based. Other studies have mapped spatial variations in river inundation area (A) as a proxy for changing stage or discharge, using visible/near-infrared or synthetic aperture radar (SAR) backscatter imagery [e.g. *Smith et al.*, 1995, 1996; *Prigent et al.*, 2001; *Brakenridge et al.*, 2005; *Papa et al.*, 2006; *Smith and Pavelsky*, 2008; *Khan et al.*, 2011]. However, these methods typically require ancillary data (e.g. from stream gages or digital elevation models (DEMs)) and are most effective for width-sensitive rivers (i.e. where discharge fluctuations are largely accommodated by changes in width). Furthermore, cloud and vegetation cover limits the use of optical sensors, while SAR backscatter techniques are limited by difficulties related to wind roughening of the water surface.

The preceding approaches measure either point-based *WSE*, or spatially-varying A, but not both. An exciting development in space-based remote sensing of river hydraulics is 3-D imaging, first advanced using repeat-pass interferometric SAR (InSAR) to measure relative changes in *WSE* over time and space [e.g. *Alsdorf et al.*, 2000, 2001, 2007a; *Lu et al.*, 2005; *Jung and Alsdorf*, 2010; *Jung et al.*, 2010]. This approach can detect temporal changes in *WSE* to a vertical precision of several centimeters, but requires inundated vegetation for signal return and only measures relative changes (i.e. height anomalies, $\mathrm{d}WSE/\mathrm{d}t$) over time for a particular location. Hydraulic surface slopes, for example, cannot be mapped with this method. Therefore while repeat-pass InSAR, like profiling altimetry and inundation mapping, demonstrates the vast potential of remote sensing for studying 3-D river dynamics, no sensor currently exists to quantify terrestrial surface water elevations, storages, and fluxes globally over time and space [*Alsdorf et al.*, 2007b; *Durand et al.*, 2010b].

The NASA Surface Water and Ocean Topography (SWOT) satellite, planned for launch in 2019, has strong potential to overcome many of the aforementioned limitations to space-based

measurements of river systems. Using Ka-band wide-swath radar interferometry, SWOT will provide unprecedented worldwide measurements of terrestrial and coastal waters [*swot.jpl.nasa.gov*]. Through instantaneous detection of both *WSE* and *A*, SWOT will provide global 3-D imaging of river hydraulics, as well as topographic mapping of exposed river bathymetry (i.e. any portion of the river channel that happens be exposed above *WSE* at the time of a satellite overpass) and surrounding floodplains for rivers wider than ~100 m. Owing to very bright returns of near-nadir Ka band radar, global, repeated measurements of *A* and effective width (W_e, inundation area/reach length) will be obtained with repeat intervals ranging from 2 to 11 days depending on latitude. Furthermore, because SWOT will have two radar antennas the requirement of repeat-pass interferometry is overcome, thus allowing instantaneous acquisition of spatial fields of *WSE*, from which water surface slopes can also be derived.

While global measurements of terrestrial *WSE* and water surface slope will have numerous scientific and practical applications, they do not represent direct measurements of river discharge (m^3/s). Global knowledge of discharge would, for instance, greatly improve the ability to quantify the availability and fluxes of surface water, especially in remote or developing regions. However, unless the full channel bathymetry is either independently known or observed (i.e. the river dries up completely) at least once over the SWOT mission lifetime, the depth of river flow below the free-water surface remains unknown. This unknown flow depth is a critical obstacle to estimating river discharge from SWOT or other remotely-sensed measurements.

Attempts to estimate river depth from remotely sensed information are few in number. Several studies have exploited the attenuation of bottom reflectance in optical imagery to estimate river bathymetry [e.g. *Legleiter et al.*, 2004, 2009; *Marcus and Fonstad*, 2008; *Legleiter and Roberts*, 2009], but spectral scattering from suspended sediment limits this approach to

clear, shallow streams where channel bottom reflectance is evident. Others have explored data assimilation techniques that combine simulated measurements of *WSE* with a hydrodynamic model to solve for depth and discharge simultaneously [e.g. *Andreadis et al.*, 2007; *Durand et al.*, 2008; *Biancamaria et al.*, 2011]. However, this approach requires both implementation of a hydrodynamic model and *a priori* estimates of input variables such as channel bathymetry and roughness that are not commonly available. Another approach [*Durand et al.*, 2010b] estimates stream depth using an algorithm based on Manning's equation, but this approach assumes an unrealistic rectangular cross-section and requires independent estimation of the Manning's roughness coefficient from ancillary data.

Few studies have explored this depth-estimation problem from a purely geomorphological standpoint. Using a large dataset compiled from U.S. Geological Survey cross-sections, *Bjerklie* [2007] developed a simple regression equation to estimate bankfull mean depth (d_{bf}, the mean depth at bankfull discharge) from observed values of bankfull width and channel slope. This equation produced a large standard error of ~58%, leading the authors to call for "improved methods to estimate bankfull depth from observed variables" [*Bjerklie*, 2007].

One such method (for estimating river depth solely from remotely sensed measurements) is to exploit empirical relationships between co-varying, interrelated hydraulic variables (i.e. *WSE* and W_e), where stable relationships can be found, to estimate a third variable (i.e. unobservable flow depth). Identification of these empirical relationships has been a central theme in fluvial geomorphology for decades, both at single locations (called "at-a-station hydraulic geometry") and between different locations ("downstream hydraulic geometry") along a river. Classic hydraulic geometry (HG) theory describes the empirical relationships of width (w), depth (d), and velocity (v) with discharge (Q) expressed as the simple power functions $w=aQ^b$, $d=cQ^f$,

and $v=kQ^m$, where *a, b, c , f, k, and m* are empirical constants unique to a particular river cross-section and/or downstream locations [*Leopold and Maddock*, 1953]. Because $Q=wdv$, the exponents b, f, and m essentially describe the "trade-offs" between flow width, depth, and velocity (i.e. $b+f+m=1$), caused mainly by the shape of a stream channel at a given location. Where stable HG relationships exist, they form the basis for stream gage discharge estimates through construction of an empirical *WSE*-discharge relationship (rating curve) relating occasional *in situ* measurements of discharge to continuous measurements of *WSE*. For locations that are depth-sensitive (i.e. where changes in discharge are significantly accommodated by adjustments in flow depth) and flows are normally confined within the channel banks, *WSE* thus becomes a reliable proxy for discharge.

Stable at-a-station HG relationships have long been identified in field measurements, and it now appears possible to also observe them from space [*Smith and Pavelsky*, 2008]. This suggests that remotely sensed *WSE* and W_e may be useful for estimating certain hydraulic properties of river channels. In principle, even discharge could be retrieved for a few specific locations (where in situ measurements could be simultaneously collected for calibration) but numerous studies have documented the highly variable nature of HG relationships along a river course [e.g. *Leopold and Maddock*, 1953; *Richards*, 1973; *Knighton*, 1975; *Park*, 1977] meaning that such functions, once derived, are non-transferable to other locations. A major uncertainty in adapting at-a-station HG to a remote sensing context is determining how HG relationships, normally derived for river cross-sections, are influenced by "reach-averaging" (i.e. spatial averaging over some planimetric river area, called reach length) that is necessary when using image data [*Smith and Pavelsky*, 2008]. SWOT retrievals of *WSE*, in particular, will be spatially averaged over reach lengths of tens to hundreds of meters in order to improve the precision of its

WSE retrieval [*Durand et al.*, 2010a]. The implications of this amount of reach-averaging for deriving empirical HG relationships from geospatial data are not well understood, with very few studies examining this question to date [*Stewardson*, 2005; *Smith and Pavelsky*, 2008; *Fonstad and Marcus*, 2010].

Even at a single location, variability in HG relationships is common, particularly for high versus low-flow conditions [*Lewis*, 1966; *Richards*, 1976; *Jowett*, 1998]. Indeed, *Lewis* [1966] highlights the substantial "slope-breaks" in HG power-law relationships that often occur at low-flows, suggesting that HG relationships calibrated at moderate-to-high flow levels can thus lead to large errors when extrapolated to low-flows. Instead of a single stable power law relating each hydraulic variable (i.e. w, d, and v) to discharge, his study found that in-channel HG relationships can often be described by two different functions, one for moderate-to-high flows and one for low-flows. Thus, from a remote sensing perspective, a W_e-*WSE* relationship derived from observations of moderate-to-high in-channel flows might be expected to lead to large errors when extrapolated to low-flows. Likewise, if a sensor could selectively observe the W_e-*WSE* relationship for low-flows, such measurements might provide more useful information for estimating unobserved hydraulic parameters (e.g. flow depth) than the same location imaged during high-flows. For those locations along a river where a stable low-flow relationship between *WSE* and W_e could be detected (through repeat-pass observations of *WSE* and W_e), this relationship could then be extrapolated to the unobserved portion of the river channel to estimate the minimum channel elevation (z_{min}) and mean flow depth (d).

The objective of this study is to explore the feasibility of estimating unobservable river depth d from remotely sensed measurements of water surface elevation *WSE*, cross-sectional flow width w, and effective width W_e alone. To do this, we generate synthetic values of *WSE*,

and w through data extraction from 1,495 field-surveyed cross-sections compiled for the Ganges-Brahmaputra, Rio Grande, Illinois, and Upper Mississippi river systems, and WSE and W_e from a continuously gridded sonar-derived bathymetric dataset for an overlapping 62 km reach of the Upper Mississippi. For the Rio Grande and Upper Mississippi rivers, synthetic values of WSE and w are also generated using the Hydraulic Engineering Center – River Analysis System (HEC-RAS) version 4.1.0 (http://www.hec.usace.army.mil/software/hec-ras/) 1-D hydraulic model, developed and distributed by the U.S. Army Corps of Engineers (USACE), thus allowing the results to be presented as a function of flow exceedance probability [*Dingman*, 2002]. These generated datasets of WSE vs. w (or W_e) are then used to explore two simple methods for estimating d from remotely sensed width-WSE relationships. The Linear Method extrapolates observed width-WSE relationships to estimate d at locations where a strong linear correlation between these two variables is observed. The Slope-break Method, motivated by *Lewis* [1966], extrapolates low-flow width-WSE relationships to estimate d only at locations where two strong linear correlations are observed, one for moderate-to-high and one for low-flows. These two methods are assessed for both the prevalence (i.e. number) of locations that are useable and the quality of the derived depth estimates for each approach. Finally, the effects of reach-averaging are studied using the continuously gridded dataset for the upper Mississippi River, to evaluate the utility of spatially-averaged W_e-WSE relationships that would be detected by SWOT and other remote sensing approaches.

2. Methods

2.1 Data and Study Areas

A total of 1,495 previously collected field-surveyed cross-sections and one continuous gridded bathymetric dataset were compiled from various sources for six tributary rivers of the Ganges-Brahmaputra system, Bangladesh [*www.iwmbd.org*], and reaches of the Rio Grande River, USA [*Tetra Tech*, 2005], Illinois River, USA [*U.S. Army Corps of Engineers*, 2004], and Upper Mississippi River, USA [*U.S. Army Corps of Engineers*, 2004]. Viewed collectively, these four study areas represent a wide range of rivers in terms of their size (~50 m - 18,000 m wide) and discharge (~1 m/s^3 – 50,000 m/s^3). The locations of the datasets and study areas are shown in Figure 1.

Each cross-section in the database consists of a transect of x and z values (distance perpendicular to the direction of flow and distance above sea level, respectively) surveyed at a particular location along the river. A total of 224 cross-sections were surveyed by the Institute of Water Modeling (IWM) along seven tributary rivers of the Ganges-Brahmaputra system (the Brahmaputra, Ganges, Jamuna, Padma, Surma, Upper Meghna, and Lower Meghna rivers) in Bangladesh. The Ganges-Brahmaputra river system constitutes one of the largest in the world, with a mean discharge on the order of 40,000 m^3/s and channel widths >10 km in places. Much of this river system is anastomosing, with wide, multi-threaded channels interspersed with permanent and shifting islands. A total of 150 cross-sections were surveyed by Tetra Tech, Inc. along ~172 km of the Rio Grande River from the Caballo Dam in southern New Mexico to the American Dam near the U.S./Mexico border. This section of the Rio Grande is located in a semi-arid environment, surrounded primarily by farmland, and is regulated by the upstream Caballo

Dam and reservoir. Mean discharge for this stretch of the Rio Grande is ~20 to 30 m^3/s and channel widths range from ~30 to 130 m. A total of 482 cross-sections were surveyed by the USACE over ~338 km of the Illinois River. The Illinois lies in a relatively temperate climate, surrounded mostly by farmland, and regulated by a series of locks and dams. Mean discharge along this reach ranges from roughly ~280 m^3/s upstream to 1000 m^3/s downstream, with channel widths ranging from ~70 to 3,300 m. A total of 639 cross-sections were surveyed by the USACE over ~315 km of the Upper Mississippi upstream of its confluence with the Ohio River. The Upper Mississippi has a temperate climate, is surrounded largely by farmland, and is regulated by a series of locks and dams. Discharge along this reach averages between ~6,000 and 7,000 m^3/s and channel widths range from ~200 to 2,300 m. An overlapping, continuously gridded (5 x 5 m) bathymetric dataset, obtained primarily from depth soundings and supplemented with manual measurements using a calibrated sounding pole was also obtained for a ~62 km river reach of this river [http://www.umesc.usgs.gov/aquatic/bathymetry/download.html]. This continuously gridded bathymetric dataset was adjusted to a constant reference water surface by the developers of the dataset, thus removing water surface slope while preserving the shape of the channel [http://www.umesc.usgs.gov/documents/bathymetry/methods.pdf].

2.2 Extraction of Synthetic Width and *WSE* Values

Synthetic values of water surface width w (for cross-sections) and effective width W_e (for gridded Upper Mississippi data) and *WSE* were extracted to test two methods for estimating d. All cross-sectional and bathymetric data were read into Matlab® version R2010a for extraction of data values. Cross-sections near bridges or dams were excluded from analysis. These synthetic values of w, W_e, and *WSE* were generated in three ways as follows.

For each of the 1,495 cross-sections, values of w and WSE were extracted as a function of channel depth, corresponding to percentages of bank-full depth d_{bf} ranging from 100% to 5% in increments of 5%, with d_{bf} visually determined at each cross-section by selecting the highest surveyed elevation that could be confidently determined as in-channel. At locations where multiple channels were encountered along the same surveyed transect (primarily along the anastomosing Ganges-Brahmaputra river system) their widths were summed together. These synthetic values of w and WSE allow for exploration of width-WSE relationships as a function of percentage channel exposure (i.e. the percentage of the channel at a given location that is exposed to a passing sensor over time).

To estimate the probability that the necessary channel exposures might actually occur over a typical 3-5 year satellite mission lifetime, a second dataset of synthetic width-WSE observations was generated using HEC-RAS to simulate real-world discharges along the Rio Grande and Upper Mississippi rivers. The necessary inputs and parameters were previously defined for these particular rivers by their respective developers [*Tetra Tech*, 2005; *U.S. Army Corps of Engineers*, 2004]. For the Upper Mississippi River, this modeling was restricted to the downstream 430 of 639 cross-sections owing to excessive influence of man-made structures on the HEC-RAS simulations. For each river, a range of steady-state flows ranging from 80% to 5% exceedance probability was simulated and the corresponding values of w, d, and WSE extracted from the surveyed cross-sections. These exceedance probabilities were determined using ten years (2001 – 2010) of daily discharge records from four USGS gaging stations along the Upper Mississippi River and one along the Rio Grande River (Figure 1).

Synthetic reach-averaged values of W_e and WSE were extracted from the Upper Mississippi bathymetric dataset in order to study the effects of reach-averaging on remotely

sensed hydraulic relationships. For ease of processing the gridded data were first discretized into 12,788 5 m sections using the USACE HEC-GeoRAS extension for ArcGIS®. Each section thus represents the average bathymetry of a 5 m reach length. Synthetic measurements of W_e and *WSE* were then extracted from these 12,788 sections in much the same manner as for the cross-section database, except the reference d_{bf} was defined as the highest recorded elevation for each section instead of from visual inspection (unlike the surveyed cross-sections, the bathymetric data do not extend onto the river floodplain). Synthetic values of W_e and *WSE* were extracted from each section at water levels corresponding to percentages of d_{bf} ranging from 100% to 5%, then spatially averaged for reach-lengths of 50 m, 100 m, 500 m, and from 1000 m to 10,000 m in increments of 1000 m. Unlike traditional surveyed cross-sections, these synthetic, reach-averaged W_e and *WSE* values derived from continuous geospatial bathymetric data enable assessment of how spatial averaging of remotely sensed observations may influence hydraulic width-*WSE* relationships in natural river systems.

2.3 Linear Method for Depth Estimation

The simplest method for estimating river depth from remotely sensed width and *WSE* is linear extrapolation of the empirical width-*WSE* relationship, constructed using all available observations acquired above the lowest observed water level (WSE_{min}). This assumes a fixed correlation between flow width and mean depth as would occur in a perfectly triangular cross-section (Figure 2, top row). It is also analogous to the classic at-a-station HG assumption of a stable power-law relationship between any of *w*, *d*, *v*, with *Q* at a given cross-section, except a linear model is used owing to no incorporation of *Q*.

To test this simplest approach, the derivatives of *WSE* with respect to *w* (d*WSE*/d*w*) were first calculated between all simulated in-channel water surfaces above a given WSE_{min} for each cross-section in the compiled database. Those locations where all observed values of d*WSE*/d*w* were within +/- 0.015 of each other were flagged. This value was chosen in order to select for locations with strongly correlated width-*WSE* relationships, while still retaining a sufficient number of cross-sections from the sample pool for which to estimate depth. For all locations satisfying this criterion ("optimal locations"), the mean of the derivatives of *WSE* with respect to *w* ($\overline{\mathrm{d}WSE/\mathrm{d}w}$) for all water surfaces above WSE_{min} was extrapolated to compute the minimum channel elevation (z_{min}), the elevation at which w=0. Next, z_{min} was subtracted from WSE_{min} to compute the maximum depth (d_{max}) then halved to compute an estimate of d (d_{est}) (given the perfectly linear relationship between width and *WSE* that this method assumes, $d_{est} = d_{max}/2$ for any given *WSE*). An example of an optimal location detected by the Linear Method is displayed in Figure 3.

The Linear Method was tested for all cross-sections in the compiled database. For those cross-sections satisfying the algorithm's linear fit requirement (optimal locations), the resultant depth estimates d_{est} were compared with true d (for a given WSE_{min}) to assess the accuracy of this approach. Repeating this process for a range of possible WSE_{min} values (i.e. from 80% to 5% of d_{bf}), reveals how width-*WSE* relationships may vary as a function of river channel exposure.

2.4 Slope-break Method for Depth Estimation

An obvious limitation of the Linear Method is that hydraulic relationships determined at moderate-to-high flows are not always appropriate for low-flows, owing to hydraulic geometry "slope-breaks" described earlier [*Lewis*, 1966]. This suggests that restricting the described linear

extrapolation only to low-flow width-*WSE* relationships, if they can be clearly discerned from moderate-to-high flow width-*WSE* relationships, may improve the derived estimates of z_{min} and d_{est}. To test this idea, a second depth-estimation algorithm was developed that selects for slope-break locations only where a distinct low-flow width-*WSE* relationship can also be detected, and then extrapolated to estimate z_{min} and d_{est}. This assumes two stable width-*WSE* relationships at a given location along a stream channel such as would occur in a trapezoidal channel (Figure 2, bottom row). In this context, "slope-break" refers to the break in slope of a line fit through a scatterplot of width vs. *WSE* at locations where two distinct hydraulic relationships exist (e.g. Figure 4). This slope-break defines the *WSE* at which the set of hydraulic relationships defined for moderate-to-high flows is replaced by a new set of hydraulic relationships defined for low-flows.

For each cross-section along each river, d*WSE*/d*w* values were first calculated from each cross-section in the database for all synthetic water surfaces above a given WSE_{min}. $\overline{\mathrm{d}WSE/\mathrm{d}w}$ was calculated from four of the highest water surfaces at each cross-section (the number of observations for calculating $\mathrm{d}WSE/\mathrm{d}w$ was arbitrarily chosen; this value had little effect on the results) and was then used to compare each subsequent (i.e. at lower elevation) value of d*WSE*/d*w*. If a subsequent value of d*WSE*/d*w* deviated sufficiently from $\overline{\mathrm{d}WSE/\mathrm{d}w}$ (a d*WSE*/d*w* value $<0.3*\overline{\mathrm{d}WSE/\mathrm{d}w}$), the cross-section was flagged as having a slope-break. Otherwise, $\overline{\mathrm{d}WSE/\mathrm{d}w}$ was recalculated to include the subsequent value of d*WSE*/d*w* and the process continued until all values were compared. Note that the value 0.3, which defines the threshold for what constitutes a slope-break, was chosen through simple trial and error, but the value of this threshold did not have much effect on results. For cross-sections where a slope-break was detected, d_{est} was only estimated at those locations where all values of d*WSE*/d*w* below the

slope-break and above WSE_{min} remained consistent with each other (i.e. within +/- .015, as for the Linear Method). Extrapolation of $\overline{\mathrm{d}WSE/\mathrm{d}w}$ to w=0 below this break was then used to estimate z_{min} and d_{est} as before. An example of an optimal location detected by the Linear Method is displayed in Figure 4.

The Slope-break Method was tested for all cross-sections in the compiled database. For those cross-sections satisfying the algorithm's criteria (optimal locations) resultant values of d_{est} were compared with true d (for a given WSE_{min}) to assess the accuracy of this approach. As with the Linear Method, this process was repeated for a range of possible WSE_{min} values (i.e. from 80% to 5% of d_{bf}), to assess how width-*WSE* relationships may vary as a function of river channel exposure. Results were compared with those of the Linear Method for each river (Figure 7). This initial comparison of the two methods made clear that the Slope-break Method outperformed the Linear Method for all rivers, thus further testing was limited to the Slope-break Method alone. The Slope-break Method was further tested on HEC-RAS-generated water surface profiles for reaches of the Rio Grande and Upper Mississippi rivers. Finally, the Slope-break method was tested on synthetic measurements extracted from the Upper Mississippi gridded bathymetric dataset for a range of reach-averaging length scales.

3. Results

3.1 Depth Estimations from Exposed Channel Cross-sections Using the Linear Method

Depth estimation errors from testing the Linear Method on all 1,495 surveyed cross-sections are plotted log-linearly in Figure 5 as a function of the percentage of channel exposed over time. Each blue symbol represents the standard error of the derived d_{est} (percent error

relative to d_{bf}) at a particular optimal location detected for a given percentage of channel exposure. The full range of standard errors in d_{est}, depending on the percentage of channel exposure (20% - 95%), is 0.02 – 2163%, 0.02 – 4024%, 11 – 3768%, and 0.005 – 604% for the Upper Mississippi, Illinois, Rio Grande, and Ganges-Brahmaputra river systems, respectively. The root mean squared error (RMSE) for all optimal locations detected for a given percentage of channel exposure is plotted in red and ranges from 11 – 302%, 18 – 377%, 760 - 1288%, and 7 – 109% for the Upper Mississippi, Illinois, Rio Grande, and Ganges-Brahmaputra river systems, respectively, depending on the percentage of channel exposure (20% - 95%). For all four river systems, both d_{est} RMSE and the number of optimal locations detected tend to decrease with increasing channel exposure. The reasons for this are discussed in section 4. For example, at 20% channel exposure 942 (63%) of the total 1,495 cross-sections were detected as optimal locations, while only 166 (11%) were detected as optimal locations at 95% channel exposure. Optimal locations were detected at all levels of channel exposure (20% - 95%) for all rivers except the Rio Grande, for which optimal locations were only detected at levels of channel exposure $\leq$70%. Thus, there were no cross-sections along the Rio Grande where dWSE/dw values remained adequately stable for channel exposures exceeding ~70%.

3.2 Depth Estimations from Exposed Channel Cross-sections Using the Slope-break Method

Depth estimation errors from testing of the Slope-break Method on all 1,495 cross-sections are plotted in Figure 6 as a function of the percentage of channel exposed over time. The full range of standard errors in d_{est}, depending on the percentage of channel exposure (20% - 95%), is 0.004 – 51%, 0.03 – 46%, 0.05 – 15%, and 0.25 – 87% for the Upper Mississippi, Illinois, Rio Grande, and Ganges-Brahmaputra river systems, respectively. The RMSE for all

optimal locations detected for a given percentage of channel exposure ranges from 3 - 20%, 4 – 35%, 2 - 8%, and 4 – 65%, for the Upper Mississippi, Illinois, Rio Grande, and Ganges-Brahmaputra river systems, respectively, depending on the percentage of channel exposure (20% - 95%). For comparison, the number of optimal locations detected and the RMSE values for both methods (Linear and Slope-break) are plotted together in Figure 7. Note the sharply reduced RMSEs and range of d_{est} errors for a given percentage of channel exposure produced by the Slope-break Method as compared with the Linear Method. As with the Linear Method, RMSE values tend to improve with increasing channel exposure for all four river systems. Unlike the Linear Method, however, the number of optimal locations detected tends to increase with increasing channel exposure. For example, at 20% channel exposure only 6 (0.4%) of the 1,495 cross-sections were detected as optimal locations, whereas 242 (16%) were detected as optimal locations at 95% channel exposure. Optimal locations were detected at all levels of channel exposure (20% - 95%) for both the Upper Mississippi and Ganges-Brahmaputra rivers and at levels of channel exposure $\geq$ 30% for the Illinois River, but $\geq$80% channel exposure was required to detect optimal locations along the Rio Grande River. Thus, the required percentage of channel exposure can vary widely between different river systems

3.3 Depth Estimations Using the Slope-break Method and HEC-RAS Simulated Water Surface Profiles

HEC-RAS simulated water surface profiles enabled study of the likelihood of slope-break exposure given historic discharge statistics. Depth estimation errors from testing of the Slope-break Method on HEC-RAS simulated water surface profiles for the Upper Mississippi and Rio Grande rivers are plotted in Figure 8 as a function of exceedance probability. The full range of standard errors in d_{est}, depending on the percentage of channel exposure (20% - 95%), is .08 –

86% and .01 – 3.60% for the Upper Mississippi and Rio Grande rivers, respectively. The RMSE for all optimal locations detected for a given exceedance probability ranges from 20 – 31% and 0.75 – 2.25% for the Upper Mississippi and Rio Grande rivers, respectively, depending on the exceedance probability value. While RMSE values tend to decrease with increasing exceedance probability (corresponding to increasing channel exposure) for the Rio Grande, a slight trend of increasing RMSE values with increasing exceedance probability is found for the Upper Mississippi. Optimal locations were detected along the Upper Mississippi for all tested exceedance probabilities (40 – 99%), while only for exceedance probabilities $\geq$58% for the Rio Grande River. Much like the previous tests on the Rio Grande and Upper Mississippi, the number of optimal locations detected tends to increase with increasing channel exposure for both rivers. For the Rio Grande, while only 2 (1.3%) of the 150 cross-sections were detected at 58% exceedance probability, 6 (4.0%) were detected at 90% exceedance probability. For the Upper Mississippi, 14 (3.3%) of 430 cross-sections were detected as optimal locations at 40% exceedance probability, while 42 (9.8%) were detected at 99% exceedance probability.

3.4 Depth Estimations Using the Slope-break Method and Synthetic Reach-averaged Values of Width and *WSE*

The continuous bathymetric dataset obtained for the Upper Mississippi River enabled study of how d_{est} values derived from geospatial data compare with those derived from surveyed transects. Depth estimation errors from testing of the Slope-break Method on synthetic reach-averaged values of width (in this case W_e) and *WSE* for 62 km of the Upper Mississippi River are plotted in Figure 9 as a function of the percentage of channel exposure. A comparison of how these errors vary with reach-averaging length is plotted in Figure 10. Optimal slope-breaks were not detected at any level of channel exposure for reach-averaging lengths >7000 m. As before,

both RMSE values and the range of errors for individual cross-sections tend to decrease with increasing channel exposure for all reach-averaging lengths at which slope-breaks were detected. Likewise, the number of optimal locations for a given reach-averaging length tends to increase with increasing channel exposure, as shown in Figure 10. As reach-averaging length increases, the number of optimal locations for a given percentage of channel exposure decreases, and a greater percentage of channel exposure is required in order for optimal slope-breaks to be detected. RMSE values for a given percentage of channel exposure remain relatively consistent at all reach-averaging lengths up to ~2000 m, but tend to increase somewhat at longer lengths. However, the range of errors for all optimal locations detected at a given percentage of channel exposure tends to decrease consistently with increasing reach-averaging length.

4. Discussion and Summary

The findings of this study suggest that remotely sensed measurements of river flow width and *WSE* alone may be useful for estimating river depth, at select locations, if a sufficient number of observations are accumulated so as to identify stable empirical correlations between the two variables. Because moderate-to-high-flow hydraulic relationships often do not extend to low-flows, a sufficient portion of a river channel's bathymetry should be observed (i.e. *WSE* must fall to sufficiently low levels) in order to identify hydraulic relationships that can be usefully extrapolated to estimate depth. The minimum amount of channel exposure necessary for the method to work varies between rivers and for different locations along the same river.

Testing of the Linear Method, for example, shows that simple linear extrapolation of W_e-*WSE* relationships observed at moderate-to-high flows can lead to highly inaccurate depth

estimates. In contrast, testing of the Slope-break Method shows that extrapolation of low-flow W_e-*WSE* relationships at locations where two distinct hydraulic relationships can be detected (one for moderate-to-high and one for low-flows) can substantially reduce this error. Indeed, the Slope-break Method showed considerable improvement in depth estimation compared to the Linear Method for all four rivers at all levels of channel exposure (Figure 7).

Although the Linear Method detected more "optimal" locations with lesser amounts of channel exposure as compared with the Slope-break Method, this seeming benefit is offset by considerably larger errors in the derived depth estimates. Indeed, as channel exposure increases the Linear Method detects fewer optimal locations, as many locations displaying "stable" *w*-*WSE* relationships at moderate-to-high flow are revealed to have unstable *w*-*WSE* relationships as more of the channel is exposed (e.g. Figure 4). While a simple linear *w*-*WSE* relationship was preserved throughout the entire range of possible *WSE*s for a small number of cross-sections, such locations could not be identified in practice unless the river channel becomes fully exposed (i.e. the river dries up) for at least one satellite overpass. Therefore, despite its apparent appeal of identifying numerous candidate locations with low amounts of channel exposure, the Linear Method's overly simplistic geomorphic assumptions (i.e. triangular channel behavior) yield poor depth-estimation results.

The Slope-break Method mitigates this weakness by selecting for locations where two linear trends in the width-*WSE* relationship are revealed instead of one. While still simplistic, this more closely reflects real-world "trapezoidal" channel geometries associated with cut banks and alluvial bar formation, as well as field-based geomorphic observations of high vs. low flow hydraulic geometries [e.g. *Lewis*, 1966; *Richards*, 1976; *Jowett*, 1998]. This also plausibly explains why the Slope-break method, in contrast to the Linear Method, tends to detect more

optimal locations with increasing channel exposure, because as *WSE* falls and submerged slope-breaks are revealed such locations become qualified for the former and disqualified for the latter. The detection of numerous slope-breaks even with channel exposures as low as 20% (e.g. the Upper Mississippi and Ganges-Brahmaputra river systems, Figure 6), is somewhat surprising given that slope-breaks were initially assumed to occur only at low-flow *WSE*s. Nonetheless, the overall conclusion drawn is that the Slope-break Method detects fewer optimal locations as compared with the Linear Method, but produced substantially smaller errors.

Reach-averaging of width and *WSE* reduces the variability in depth estimates for a given percentage of channel exposure (Figure 9), a finding which has positive implications for remotely sensed retrievals of depth. Reach-averaging does not appear to break down hydraulic relationships and may actually make them more robust by smoothing out much of the spatial variability in retrieved hydraulic variables. This acts to reduce the total number of slope-breaks detected by the Slope-break Method while increasing the robustness of those slope-breaks which are detected. That is, where slope-breaks are detected at longer reach-averaging lengths they persist for longer distances and are more reliable. This is apparent in Figure 9, where the magnitude and number of outliers and the range of depth estimate errors for a given level of channel exposure decrease drastically with increasing reach-averaging length. This finding agrees with *Smith and Pavelsky* [2008], who found that remotely sensed HG b-exponents reached stable values at reach-averaging lengths ~2-3 times the valley width. Indeed the best results for the Upper Mississippi occur at ~1000-2000 m reach-averaging lengths, which is roughly 2-3 times the mean bankfull channel width along this river reach.

The improvements in depth estimation resulting from reach-averaging of hydraulic variables is especially promising in the SWOT context, given the improvement in its *WSE*

measurement precision associated with greater spatial averaging of the returned radar echoes. Furthermore, the HEC-RAS simulations performed here for the Rio Grande and Upper Mississippi rivers suggest that the temporal sampling of most spaceborne sensors, including the planned 2-11 day return interval of SWOT, is more than sufficient to observe necessary amounts of channel exposure during a 3-5 year mission lifetime. Even for the Slope-break Method, realistic HEC-RAS simulations of typical flows on the Upper Mississippi and Rio Grande rivers suggest that their water levels are commonly low enough to expose slope-breaks approximately 60% and 42% of the time (Figure 8). Thus, the findings of this study suggest that useful depth retrievals can be obtained even given the spatial and temporal constraints of spaceborne observations.

This study was limited by the availability of adequate data used to generate synthetic water surface observations. Cross-sections only provide an approximation of remotely sensed measurements, and only at discrete and relatively sparse locations. Furthermore, the bathymetric data used in this analysis were constrained by the removal of *WSE* slope and lack of bankfull coverage. Even the Slope-break Method can produce sizable errors in d_{est}, varying with both channel exposure and location (Figure 6). Furthermore, it is important to point out that neither method (Linear or Slope-break) can possibly produce continuous depth estimates everywhere along a river. Instead, they identify a small subset of ideal channel locations where simple, linear correlations exist between a river's flow width and mean flow depth. Even spatially intermittent retrievals of depth, however, would be extraordinarily useful for estimating river discharge, either directly or through data assimilation into a hydrodynamic model.

Future work should include remotely sensed rather than modeled river width and *WSE* observations, particularly from AirSWOT (http://swot.jpl.nasa.gov/Airswot/), and further

exploration of the variability in remotely sensed hydraulic relationships for additional river types. Finally, while our approach requires no bathymetric or floodplain DEM, a thorough assessment of how SWOT (or other sensor) width and *WSE* measurement precisions would propagate further uncertainty to the derived depth estimates is warranted.

Despite these limitations, this study presents the first known method for estimating river flow depth solely from SWOT observations of effective width and water surface elevation. Its preliminary findings suggest that satellite observations of incomplete hydraulic information can be useful for remote estimation of river depth, and that classic HG principles have renewed relevance through adaptation for remote sensing purposes. The intermittent depth-retrievals presented here may also be useful for data assimilation to hydrodynamic models to constrain depth estimates elsewhere along a river course. Its relative simplicity is much of its appeal, and strong potential exists for using this or a similar approach as a first order river depth estimator on a global scale from satellite observations.

Figures

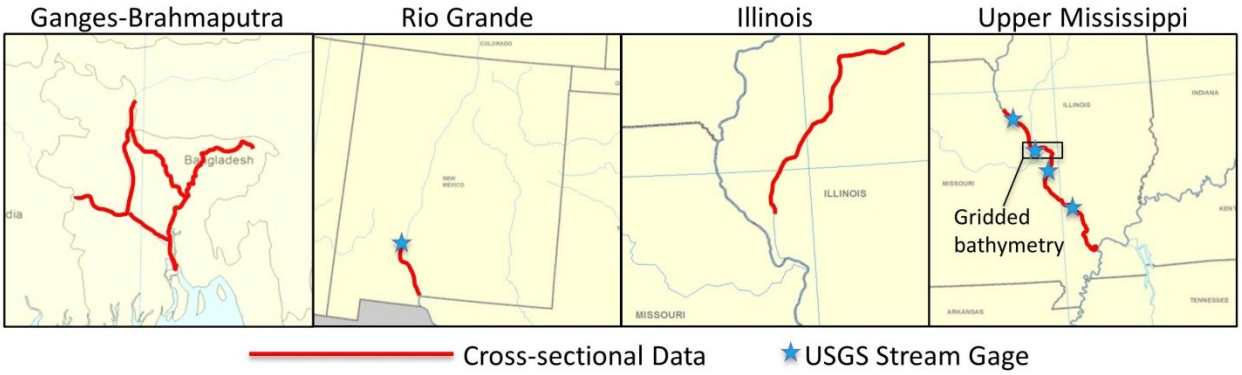

Figure 1. Location map of datasets and study areas. Cross-sectional data was attained for those river reaches highlighted in red. A black box highlights the ~62km reach of the Upper Mississippi for which gridded bathymetric data was acquired. Blue symbols mark the locations of USGS stream gages used for calculation of flow statistics.

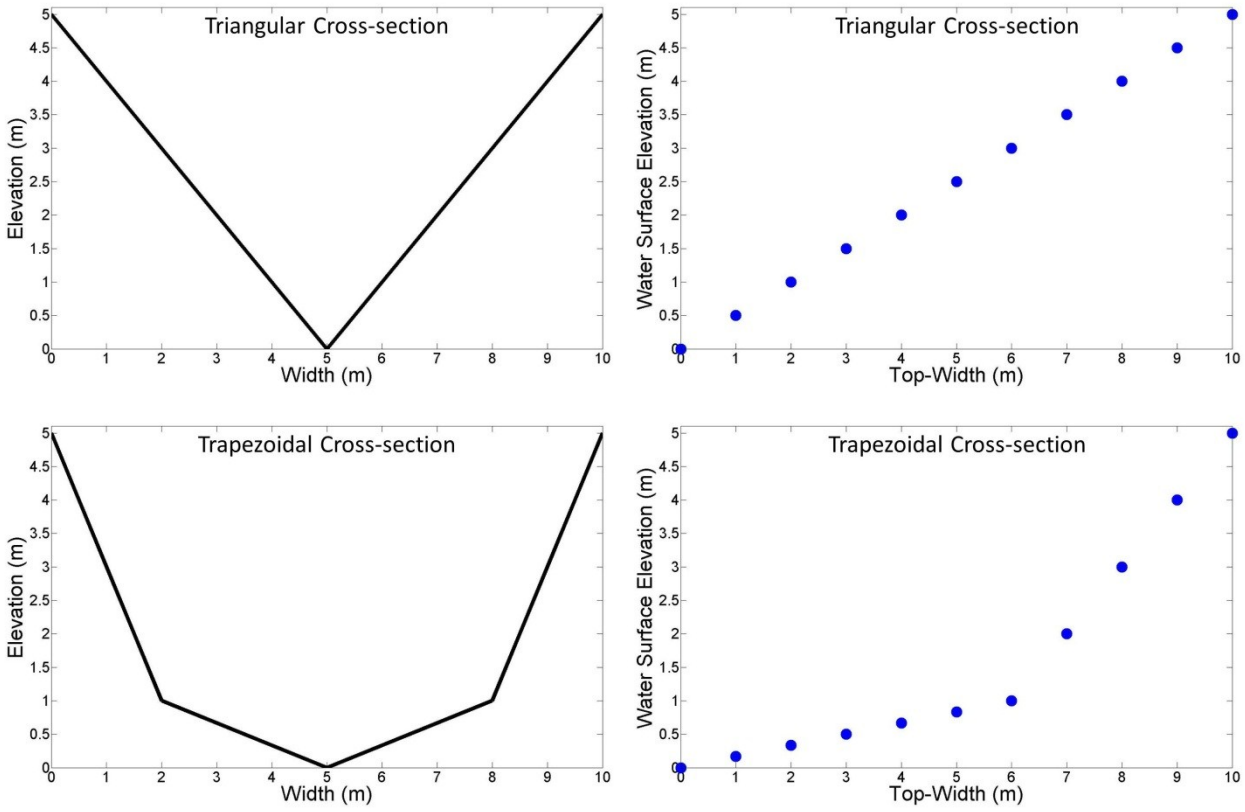

Figure 2. Two hypothetical cross-sections (left) and their respective plots of width vs. *WSE* for a range of hypothetical flow levels (right). While a single consistent width-*WSE* relationship exists for the triangular cross-section, two distinct relationships, one for moderate-to-high-flows and one for low-flows, exists for the trapezoidal cross-section.

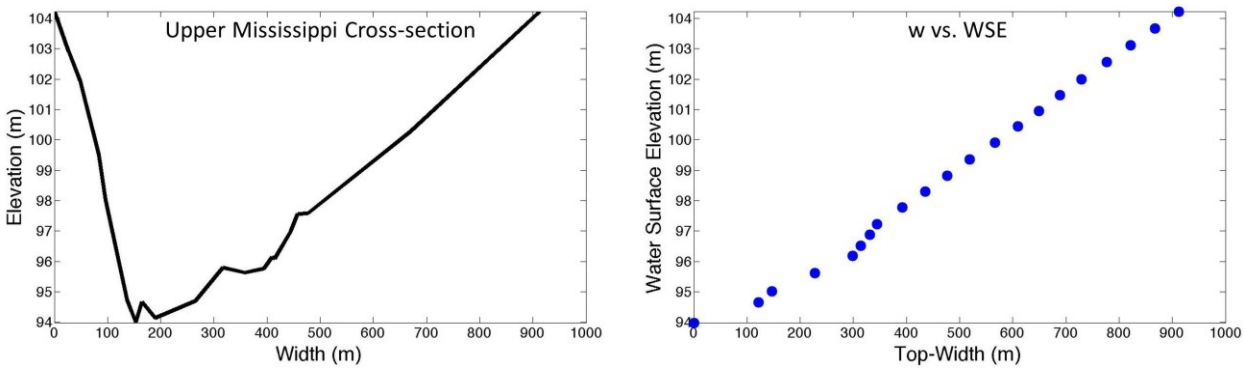

Figure 3. Example of an optimal location detected by the Linear Method. The in-channel width-*WSE* relationship remains relatively consistent with depth at this location, and thus if observed above any water level can be extrapolated to estimate z_{min} and d with reasonable accuracy.

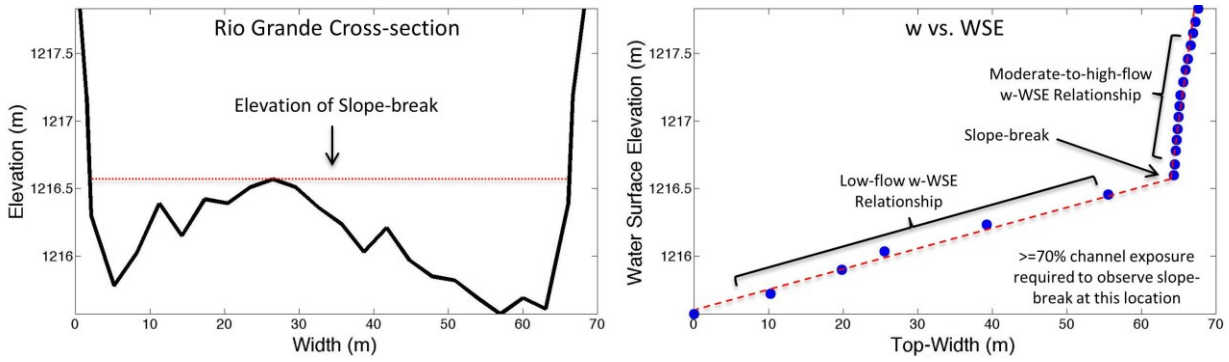

Figure 4. Example of an optimal location detected by the Slope-break Method. The cross-sectional geometry at this location results in a slope-break in the plot of width vs. *WSE* that separates two distinct in-channel width-*WSE* relationships, one for moderate-to-high flows and one for low-flows. If water levels are sufficiently low such that the slope-break is observable above the water surface (>=70% channel exposure required at this location), the low-flow width-*WSE* relationship can be extrapolated to estimate z_{min} and d with reasonable accuracy.

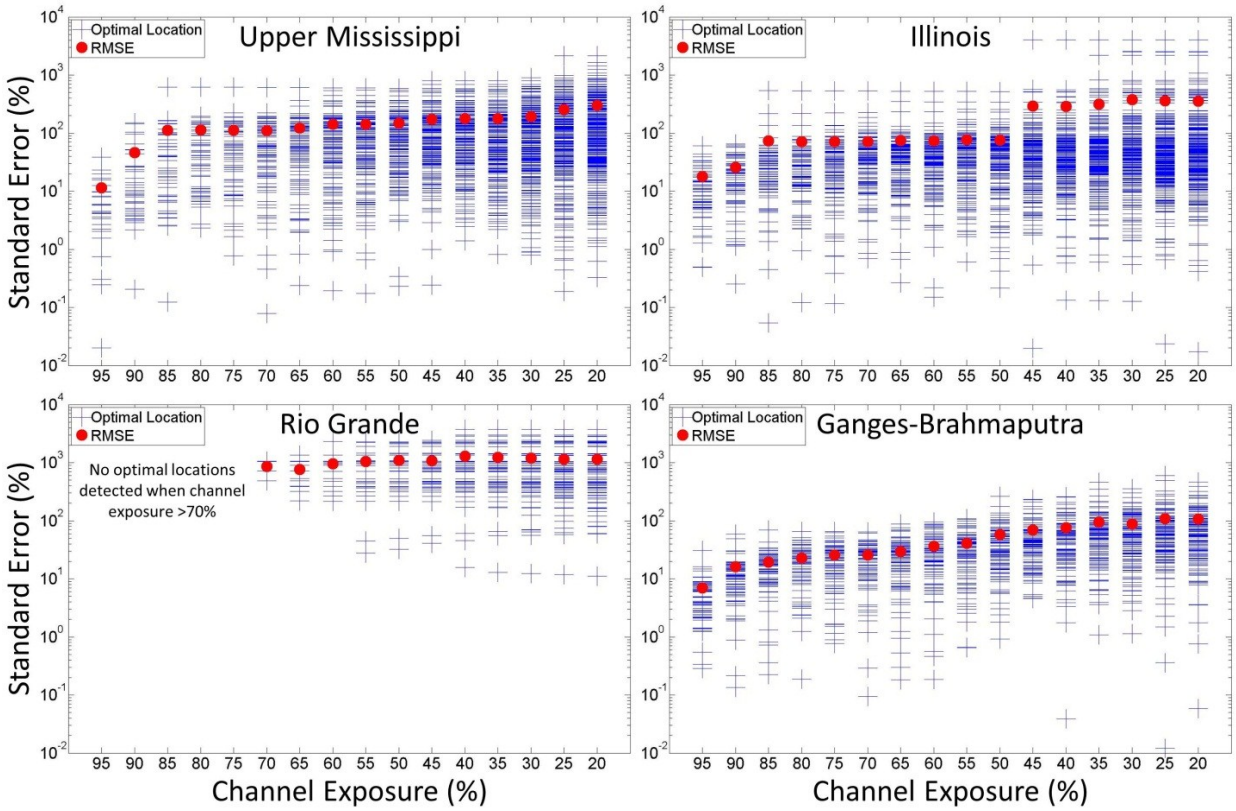

Figure 5. Results from testing of the Linear Method on synthetic values of w and WSE extracted from cross-section for four rivers. The standard error represents the percent error in d_{est} relative to d_{bf}. Each blue symbol represents the standard error at single optimal location detected at a given level of channel exposure. The RMSE for all estimates for a given percentage of channel exposure is plotted in red. In all four cases, errors tend to improve and the number of optimal locations detected tends to decrease with increasing channel exposure.

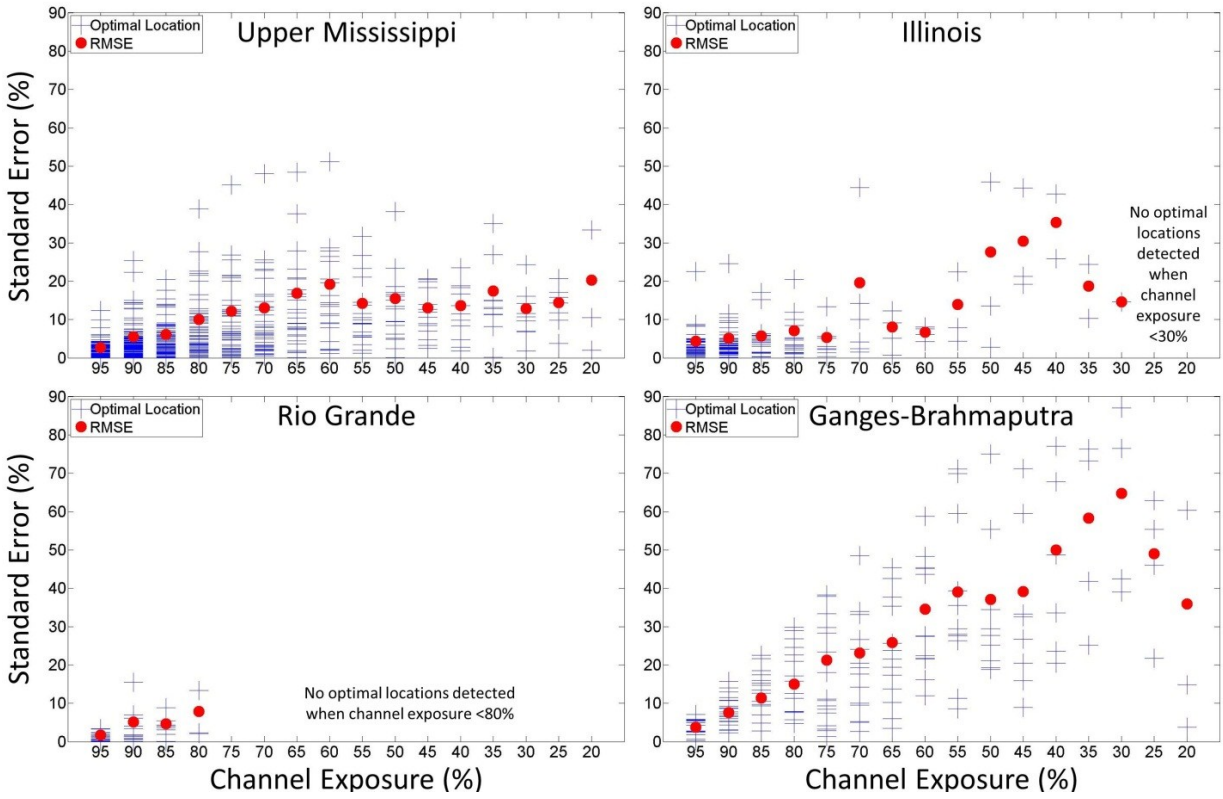

Figure 6. Results from testing of the Slope-break Method on synthetic values of w and WSE extracted from cross-section for four rivers. The standard error represents the percent error in d_{est} relative to d_{bf}. In all four cases, errors tend to improve and the number of optimal locations detected tends to increase with increasing channel exposure.

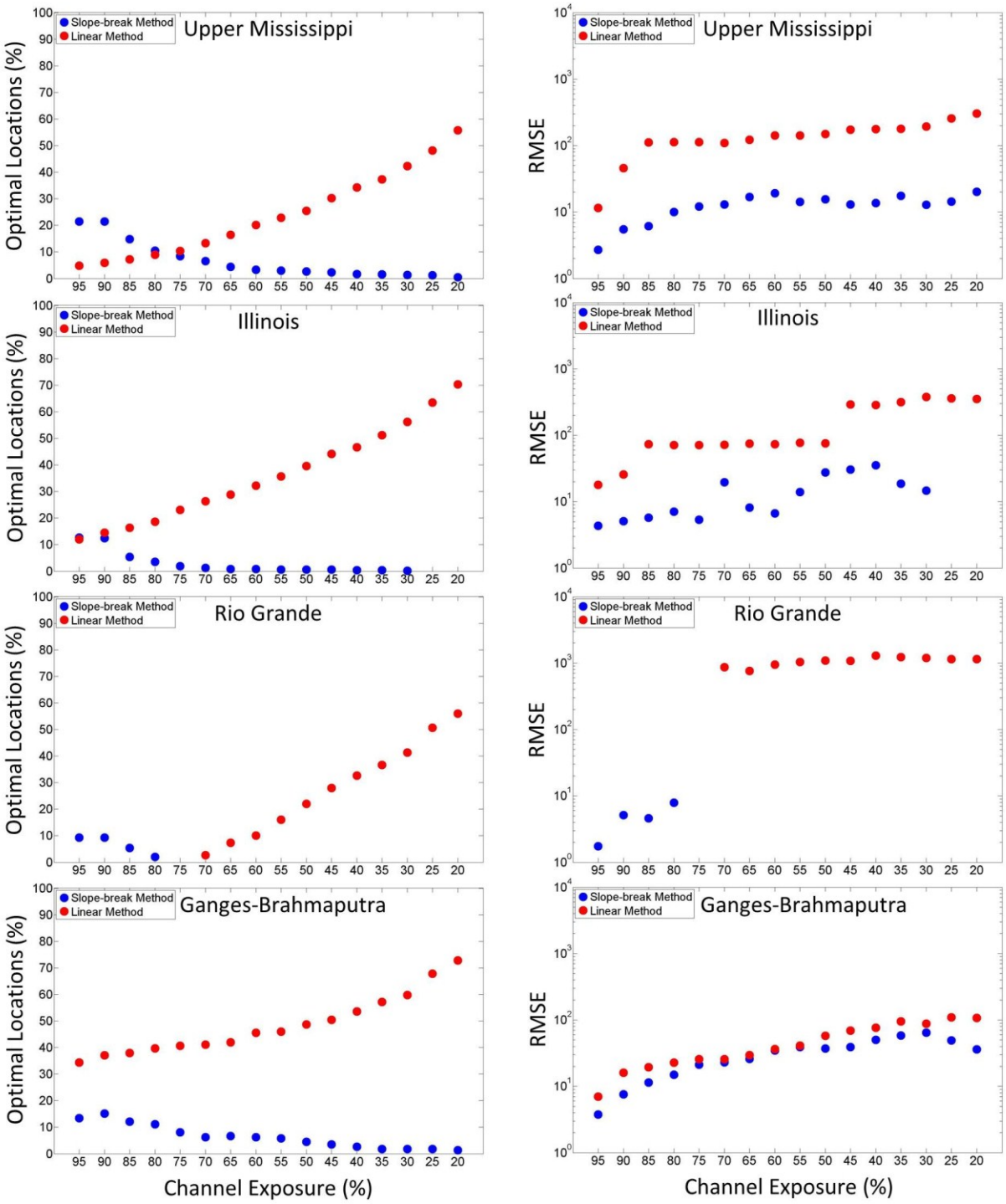

Figure 7. Comparison of the number of optimal locations detected (left column) and RMSEs (right column) for the Linear Method (red) and Slope-break Method (blue). Note the opposite trends in the number of optimal locations detected by each method, and that the Slope-break Method performed better than the Linear Method at all level of channel exposure.

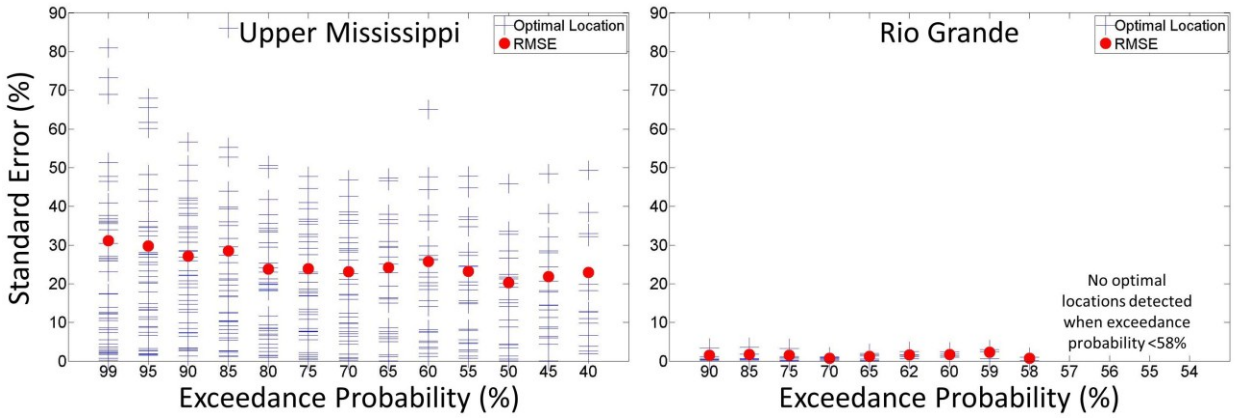

Figure 8. Results from testing of the Slope-break Method on simulated water surface observations modeled in HEC-RAS for a range of exceedance probabilities (i.e. the percentage of days a given flow is exceeded over some period of time) along two rivers. The standard error represents the percent error in d_{est} relative to d_{bf}. Slope-breaks are detected at flow-levels which are exceeded 40% and 58% of the time for the Upper Mississippi and Rio Grande rivers, respectively.

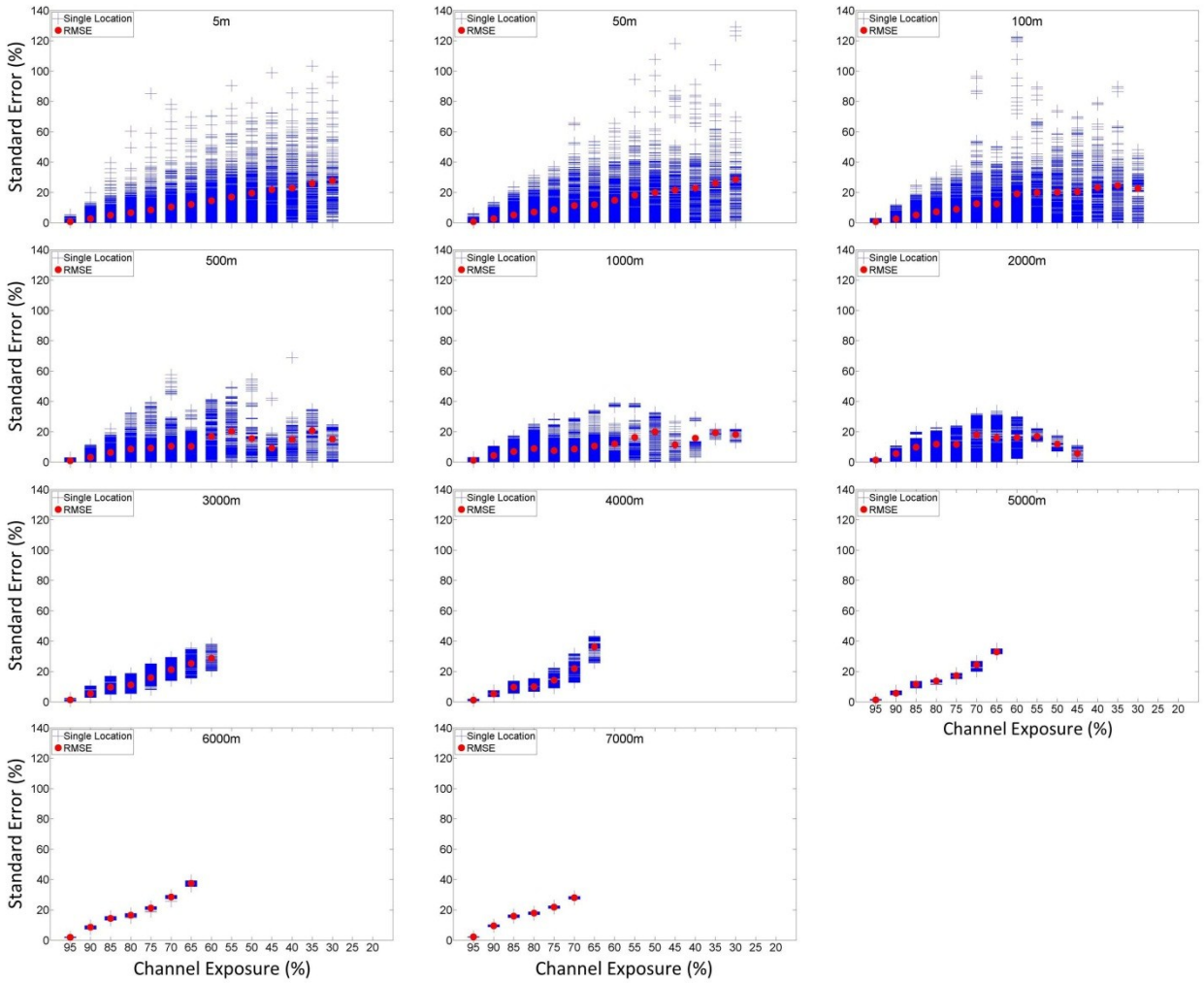

Figure 9. Results from testing of the Slope-break Method on synthetic values of W_e and *WSE* extracted along the Upper Mississippi as a function of channel depth and spatially averaged over a range of reach lengths. The standard error represents the percent error in d_{est} relative to d_{bf}. RMSE values tend to decrease with increasing channel exposure at all reach-averaging lengths. The range of errors for a given percentage of channel exposure decreases drastically with increasing reach-averaging length due to the decrease in spatial variability resulting from spatial averaging.

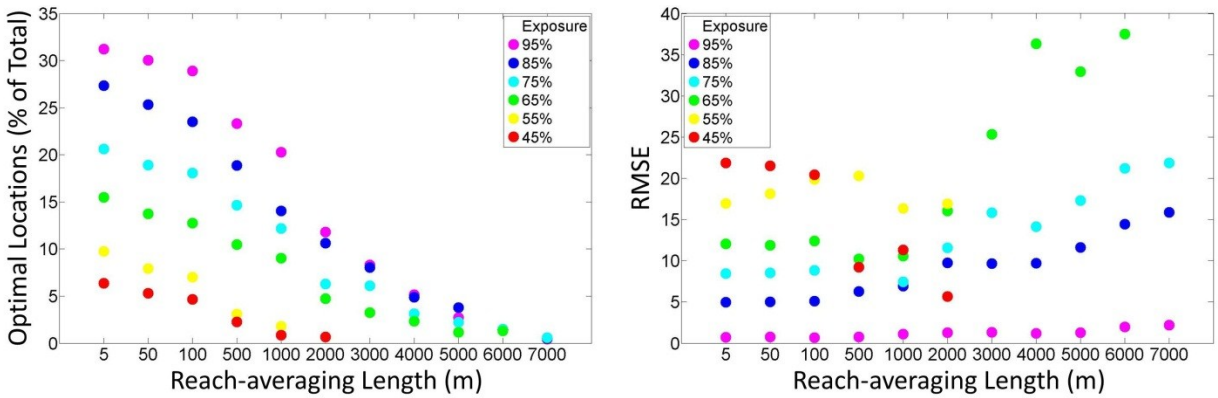

Figure 10. The percentage of cross-sections detected as optimal locations by the Slope-break Method (left) and the RMSEs for depth estimates (right) as they vary with percentage of channel exposure for a range of reach-averaging lengths. The percentage of cross-sections detected as optimal locations tends to increase with increasing channel exposure but decrease with increasing reach-averaging length. RMSE values for d_{est} tend to decrease with increasing channel exposure; they remain fairly consistent up to reach-averaging lengths of 2000 m (except at 45% channel exposure), but tend to increase at longer reach-averaging lengths.

Appendix A: Datasets Used in Study

Ganges-Brahmaputra River System Cross-section Dataset

Cross-sections were surveyed by the Institute of Water Modeling (IWM) – Bangladesh (www.iwmbd.org) in 2005 and made available through a five-year MOU between the IWM and Tennessee Technical University (TTU) [provided by Faisal Hossain (TTU) for the purposes of this study]. A total of 226 cross-sections for 7 tributaries of the Ganges-Brahmaputra river system (the Brahmaputra, Ganges, Jamuna, Padma, Surma, Upper Meghna, and Lower Meghna rivers) were acquired as a text file in HEC-RAS geometry format, as a series of point-transects along the rivers.

Rio Grande River Cross-section Dataset

Cross-sections were surveyed by Tetra Tech Inc. from 2004 to 2005 in coordination with the USACE and International Boundary and Water Commission (IBWC) as part of the Rio Grande Canalization Project (RGCP) [provided by Edward Beighley (FM Global) for the purposes of this study]. A total of 150 cross-sections were acquired as a text file in HEC-RAS geometry format, as a series of point-transects along the river. The documentation for data collection can be found in a report titled "FLO-2D Model Development Below Caballo Dam URGWOM" (ftp://63.96.218.8/FLO2D_RGCP_RptOnly.pdf).

Upper Mississippi and Illinois Rivers Cross-section Datasets

Cross-sections were surveyed by the USACE as part of the Upper Mississippi River System Flow Frequency Study [provided by Edward Beighley (FM Global) for the purposes of this study]. A total of 639 cross-sections for the Upper Mississippi River and 482 cross-sections for the Illinois River were acquired as a text file in HEC-RAS geometry format, as a series of point-transects along the river.

Upper Mississippi Gridded Bathymetric Dataset

Bathymetric data was surveyed and developed by the USGS over many years starting in 1989 as part of the Long Term Resource Management Project (LTRMP) for the Upper Mississippi river system. This data was acquired primarily from depth-soundings/chart recordings in coordination with a land-based GPS positioning system and augmented by manual measurements using a calibrated sounding pole where necessary (due to complications with shallow using the boat-based depth-sounder in shallow waters). The documentation and data can be downloaded from http://www.umesc.usgs.gov/ltrmp.html.

Appendix B: Matlab Code for Linear Method and Slope-break Method

Linear Method

```
clear all; close all; clc
pcmac = 1;
river = 1;
para1 = .015;
[D,RS,W,h,npro,nsta,wh,zmin,hb,Db,Wb] = load_output(pcmac,river);
for lf = 4:npro-1
   flagxs = zeros(1,1);
   count = 1;
   for i = 1:nsta
      for ii = 2:lf
         if wh(i,ii)>=wh(i,ii-1)-para1 && wh(i,ii)<=wh(i,ii-1)+para1,
            if ii==lf, flagxs(count)=i; count=count+1; end
         else
            break;
         end
      end
   end
   if length(flagxs)==1 && flagxs==0, Derror(1,lf-3)=NaN; RMSE_Derror(lf-3)=NaN;
      num_xs(lf-3)=NaN; perc_xs(lf-3)=NaN; continue; end
   meanwh = zeros(1,1);
   Derror1 = zeros(1,1);
   for i = 1:length(flagxs)
      xs(i,lf-3) = flagxs(i);
      meanwh = mean(wh(flagxs(i),1:lf));
      Dest(i,lf-3) = (h(flagxs(i),lf+1) - (h(flagxs(i),lf+1) - W(flagxs(i),lf+1)*meanwh))/2;
      Dtrue(i,lf-3) = D(flagxs(i),lf+1);
      Ddiff(i,lf-3) = Dest(i,lf-3)-Dtrue(i,lf-3);
      Derror(i,lf-3) = (abs(Ddiff(i,lf-3))/Db(flagxs(i)))*100; Derror1(i) = (abs(Ddiff(i,lf-3))/Db(flagxs(i)))*100;
   end
   SE = Derror1.^2;
   RMSE_Derror(lf-3) = sqrt(sum(SE)/length(SE));
   num_xs(lf-3) = length(flagxs);
   perc_xs(lf-3) = (num_xs(lf-3)/nsta)*100;
end
xs(xs==0)=NaN; Dest(Dest==0)=NaN; Dtrue(Dtrue==0)=NaN; Ddiff(Ddiff==0)=NaN; Derror(Derror==0)=NaN;
Ddiff=fliplr(Ddiff); Derror=fliplr(Derror); Dest=fliplr(Dest); Dtrue=fliplr(Dtrue);
RMSE_Derror=fliplr(RMSE_Derror); num_xs=fliplr(num_xs); xs=fliplr(xs); perc_xs=fliplr(perc_xs);
if river==1, fname = 'zz_results_method1_Rio.mat'; end; if river==2, fname = 'zz_results_method1_Miss.mat'; end
if river==3, fname = 'zz_results_method1_Ill.mat'; end; if river==4, fname = 'zz_results_method1_Bang.mat'; end
save(fname, 'Derror','RMSE_Derror','xs','num_xs','perc_xs','Dest','Dtrue','Ddiff');
fig1 = figure; ss = get(0,'ScreenSize'); set(fig1,'Position',[ss(1) ss(2) ss(3) ss(4)])
p1 = semilogy(Derror','+b','MarkerSize',38);
hold on
p2 = semilogy(RMSE_Derror,'.r','MarkerSize',70);
% if river==1, t=title(' Rio Grande ', 'FontSize', 42); end; if river==2, t=title(' Upper Mississippi ', 'FontSize', 42); end;
% if river==3, t=title(' Illinois ', 'FontSize', 42); end; if river==4, t=title(' Ganges-Brahmaputra ', 'FontSize', 42); end;
% set(t,'Position',[8.5,2700,0]);
% xlabel('Channel Exposure (%)','FontSize',42)
% ylabel('Error Relative to D_b_f (%)','FontSize',42)
leg = legend([p1(end) p2(end)],'Optimal Location','RMSE','Location','NorthWest');
set(leg,'Fontsize',30)
xlim([0 npro-3])
ylim([10^-2 10^4])
set(gca,'XTick',1:1:npro-4); set(gca,'XTickLabel',95:-5:20); set(gca,'FontSize',32);
```

Slope-break Method

```
clear all; close all; clc; tic
pcmac = 2;                % pc=1, mac=2
river = 1;               % 1=rio; 2=upper_miss; 3=bangladesh; 4=Illinois; 5=LTRMP_upper_miss
initial_flows = 3;        % number of flows to take average wh from
plot_yn = 1; plottype = 2;  % plot_yn: 1=yes, 0=no;  plottype: 1:% BF WSE/W 2=HEC WSE/W (for Rio and Miss)
save_vars = 1;            % 1=yes; 0=no;
threshold = .3;
consistency = .015;
%%%%%%%%%%%%%%%%%%%%%%%%%%%%%%%%%%%%%%%%%%%%%%%%%%%%%%%%%%%%%%
% for resample_length = [5 50 100 500 1000:1000:10000]
% clearvars -except pcmac river initial_flows nflows plot_yn save_vars threshold consistency resample_length
% [D,Q,RS,W,h,npro,nsta,wh,zmin,hb,Db,Wb] = load_resample(pcmac,resample_length);
if river~=5, [D,RS,W,h,npro,nsta,wh,zmin,hb,Db,Wb] = load_output(pcmac,river); end
nflows = npro-initial_flows-1;
for flow=1:nflows
   lowflow = npro-flow;
   [test1,zmin_guess,flag_xs,flag_pro] = flag(npro,nsta,W,h,wh,lowflow,initial_flows,threshold,consistency);
   if test1==1, continue, end
            [test2,xs,pro,depth_guess] = refine_guesses(h,lowflow,flag_xs,flag_pro,zmin_guess);
   if test2==1, continue, end
   num_xs(flow) = length(depth_guess); perc_xs(flow) = (num_xs(flow)/nsta)*100;
   for i = 1:length(depth_guess)
      D_true(i,flow)=D(xs(i),lowflow+1); Db_true(i,flow)=Db(xs(i));
      flagxs(i,flow)=xs(i); D_est(i,flow)=depth_guess(i);
   end
   parameters(1,flow)=threshold; parameters(2,flow)=consistency;
end
flagxs(flagxs==0)=NaN; D_est(D_est==0)=NaN; D_true(D_true==0)=NaN; Db_true(D_true==0)=NaN;
[D_diff,RMSE_diff,D_error,RMSE_error,AME,AMedE] = errors(river,D_est,D_true,Db_true);
if save_vars==1
   if river==5, fname = ['results_LTRMP_', num2str(resample_length), 'm', '.mat'];
   else if river==1, fname = 'zHEC_results_Rio.mat'; end; if river==2, fname = 'zHEC_results_Miss.mat'; end
       if river==3, fname = 'results_Ill.mat'; end; if river==4, fname = 'results_Bang.mat'; end
   end
      save(fname, 'river','initial_flows','nflows','flagxs','num_xs','perc_xs','parameters',...
         'D_true','Db_true','D_est','D_diff','RMSE_diff','D_error','RMSE_error','AME','AMedE');
end
if plot_yn==1, Plot_Est(pcmac,river,npro,flagxs,D_diff,AME,AMedE,RMSE_diff,D_error,RMSE_error,plottype); end
toc
%end

% pcmac; 1=PC; 2=Mac
% river 1=Rio Grande; 2=Upper Mississippi; 3=Illinoi;; 4=Bangladesh; 5=LTRMP
function [D,RS,W,h,npro,nsta,wh,zmin,hb,Db,Wb,x,z] = load_output(pcmac,river)
HECyn = 0;
if pcmac == 1
   if HECyn==1
      if river == 1, load('C:\Users\mmersel\Documents\My
Dropbox\Research\Matlab\Depth_estimation\Outputs\Rio_output_HECEP.mat'); x=NaN; z=NaN; end
      if river == 2, load('C:\Users\mmersel\Documents\My
Dropbox\Research\Matlab\Depth_estimation\Outputs\Miss_output_HECEP.mat'); x=NaN; z=NaN; end
   else
      if river == 1, load('C:\Users\mmersel\Documents\My
Dropbox\Research\Matlab\Depth_estimation\Outputs\Rio_output.mat'); end
      if river == 2, load('C:\Users\mmersel\Documents\My
Dropbox\Research\Matlab\Depth_estimation\Outputs\Miss_output.mat'); end
   end
   if river == 3, load('C:\Users\mmersel\Documents\My Dropbox\Research\Matlab\Depth_estimation\Outputs\Ill_output.mat');
end
   if river == 4, load('C:\Users\mmersel\Documents\My
```

```
Dropbox\Research\Matlab\Depth_estimation\Outputs\Bang_output.mat'); end
   if river == 5, load('C:\Users\mmersel\Documents\My
Dropbox\Research\Matlab\Depth_estimation\Outputs\LTRMP_resample.mat'); end
end
if pcmac == 2
   if HECyn==1
      if river == 1, load('/Users/MKMersel/Dropbox/Research/Matlab/Depth_estimation/Outputs/Rio_output_HECEP.mat');
x=NaN; z=NaN; end
      if river == 2, load('/Users/MKMersel/Dropbox/Research/Matlab/Depth_estimation/Outputs/Miss_output_HECEP.mat');
x=NaN; z=NaN; end
   else
      if river == 1, load('/Users/MKMersel/Dropbox/Research/Matlab/Depth_estimation/Outputs/Rio_output.mat'); end
      if river == 2, load('/Users/MKMersel/Dropbox/Research/Matlab/Depth_estimation/Outputs/Miss_output.mat'); end
   end
   if river == 3, load('/Users/MKMersel/Dropbox/Research/Matlab/Depth_estimation/Outputs/Ill_output.mat'); end
   if river == 4, load('/Users/MKMersel/Dropbox/Research/Matlab/Depth_estimation/Outputs/Bang_output.mat'); end
   if river == 5, load('/Users/MKMersel/Dropbox/Research/Matlab/Depth_estimation/Outputs/LTRMP_resample.mat'); end
end
end

%flag cross-sections that meet criteria
function [test1,zmin_guess,flag_xs,flag_pro] = flag(npro,nsta,W,h,wh,lowflow,initial_flows,threshold,consistency)
flag_xs = zeros(1,1); flag_pro = zeros(1,1); zmin_guess = zeros(1,1); xs = zeros(1,1); pro = zeros(1,1);
for iiii=1
   wh_init = mean(wh(:,1:initial_flows),2);
   % select cross-sections with significant break in wh
   count = 1;
   for i = 1:nsta
      for ii = (initial_flows+1):lowflow
         if wh(i,ii) < threshold*wh_init(i)
            xs(count) = i;
            pro(count) = ii;
            count = count+1;
            break
         else
            wh_init(i) = mean(wh(i,1:ii));
         end
      end
   end
   % if no XS are flagged, break out
   test1 = 0;
   fxs = xs;
   if length(fxs(fxs~=0))==0    %#ok<ISMT>
      test1 = 1; break
   end
   % select cross-sections with consistent dh/dw after break
   count = 1;
   for i = 1:length(xs)
      marker = 0;
      for ii = 1:(npro-pro(i)-1)
         if wh(xs(i),pro(i)+ii)>=wh(xs(i),pro(i))-consistency &&...
           wh(xs(i),pro(i)+ii)<=wh(xs(i),pro(i))+consistency
            marker = 1;
         else
            marker = 0;
            break
         end
         if ii == npro-pro(i)-1 && marker==1
            flag_xs(count,1) = xs(i);
            flag_pro(count,1) = pro(i)+1;
            mean_wh(count,1) = mean(wh(xs(i),pro(i):lowflow));
            count = count+1;
```

```
        end
      end
   end
   % if no XS are flagged, break out
   test1 = 0;
   fxs = flag_xs;
   if length(fxs(fxs~=0))==0        %#ok<ISMT>
      test1 = 1; break
   end
   % guess zmin
   zmin_guess = h(flag_xs,lowflow+1) - W(flag_xs,lowflow+1) .* mean_wh;
end
end

function [test2,xs,pro,D_est] = refine_guesses(h,lowflow,flag_xs,flag_pro,zmin_guess)
D_est = zeros(1,1);
D_init = (h(flag_xs,lowflow+1)-zmin_guess)./2;
xs = zeros(1,1);
pro = zeros(1,1);
count = 1;
for i = 1:length(D_init)
   if D_init(i)<(mean(D_init)+.25*std(D_init)) %&& D_init(i)>0
      xs(count,1) = flag_xs(i,end);
      pro(count,1) = flag_pro(i,end);
      D_est(count,1) = D_init(i,1);
      count = count+1;
   end
end
test2 = 0;
if length(xs(xs~=0))==0, test2 = 1; end
end

function [D_diff,RMSE_diff,D_error,RMSE_error,AME,AMedE] = errors(river,D_est,D_true,Db_true)
D_diff = D_true - D_est;
for i = 1:length(D_diff(1,:))
   AME(i) = mean(abs(D_diff(isnan(D_diff(:,i))==0,i)));
   AMedE(i) = median(abs(D_diff(isnan(D_diff(:,i))==0,i)));
end
for i = 1:length(D_diff(1,:))
   SE = D_diff(:,i).^2;
   SE = SE(isnan(SE)==0);
   RMSE_diff(1,i) = sqrt(sum(SE)/length(SE));
   clear SE
end
for i = 1:length(D_diff(1,:))
   D_error = (abs(D_diff)./Db_true)*100;
end
for i = 1:length(D_error(1,:))
   SE = D_error(:,i).^2;
   SE = SE(isnan(SE)==0);
   RMSE_error(1,i) = sqrt(sum(SE)/length(SE));
   clear SE
end
end
```

Works Cited

Alsdorf, D. E., et al. (2000), Interferometric radar measurements of water level changes on the Amazon flood plain, *Nature*, *404*(6774), 174-177.

Alsdorf, D. E., et al. (2001), Amazon floodplain water level changes measured with interferometric SIR-C radar, *Ieee Transactions on Geoscience and Remote Sensing*, *39*(2), 423-431.

Alsdorf, D. E., et al. (2007a), Spatial and temporal complexity of the Amazon flood measured from space, *Geophys. Res. Lett.*, *34*(8), 5.

Alsdorf, D. E., et al. (2007b), Measuring surface water from space, *Reviews of Geophysics*, *45*(2).

Andreadis, K. M., et al. (2007), Prospects for river discharge and depth estimation through assimilation of swath-altimetry into a raster-based hydrodynamics model, *Geophys. Res. Lett.*, *34*(10).

Biancamaria, S., et al. (2011), Assimilation of virtual wide swath altimetry to improve Arctic river modeling, *Remote Sens. Environ.*, *115*(2), 373-381.

Birkett, C. M. (1998), Contribution of the TOPEX NASA radar altimeter to the global monitoring of large rivers and wetlands, *Water Resources Research*, *34*(5), 1223-1239.

Birkett, C. M., et al. (2002), Surface water dynamics in the Amazon Basin: Application of satellite radar altimetry, *J. Geophys. Res.-Atmos.*, *107*(D20), 21.

Birkett, C. M., and B. Beckley (2010), Investigating the Performance of the Jason-2/OSTM Radar Altimeter over Lakes and Reservoirs, *Mar. Geod.*, *33*, 204-238.

Bjerklie, D. M. (2007), Estimating the bankfull velocity and discharge for rivers using remotely sensed river morphology information, *Journal of Hydrology*, *341*(3-4), 144-155.

Brakenridge, G. R., et al. (2005), Space-Based Measurement of River Runoff, *EOS, Transactions, American Geophysical Union*, *86*(19), 185-192.

Calmant, S., et al. (2008), Monitoring Continental Surface Waters by Satellite Altimetry, *Surv. Geophys.*, *29*(4-5), 247-269.

Cretaux, J. F., and C. Birkett (2006), Lake studies from satellite radar altimetry, *C. R. Geosci.*, *338*(14-15), 1098-1112.

Dingman, S. L. (2002), *Physical Hydrology*, Second ed., Waveland Press, Inc., Long Grove, Illinois.

Durand, M., et al. (2008), Estimation of bathymetric depth and slope from data assimilation of swath altimetry into a hydrodynamic model, *Geophys. Res. Lett.*, *35*(20), 5.

Durand, M., et al. (2010a), The Surface Water and Ocean Topography Mission: Observing Terrestrial Surface Water and Oceanic Submesoscale Eddies, *Proceedings of the Ieee*, *98*(5), 766-779.

Durand, M., et al. (2010b), Estimating River Depth From Remote Sensing Swath Interferometry Measurements of River Height, Slope, and Width, *Ieee Journal of Selected Topics in Applied Earth Observations and Remote Sensing*, *3*(1), 20-31.

Fonstad, M. A., and W. A. Marcus (2010), High resolution, basin extent observations and implications for understanding river form and process, *Earth Surface Processes and Landforms*, *35*(6), 680-698.

Frappart, F., et al. (2005), Floodplain water storage in the Negro River basin estimated from microwave remote sensing of inundation area and water levels, *Remote Sens. Environ.*, *99*(4), 387-399.

Jowett, I. G. (1998), Hydraulic geometry of New Zealand rivers and its use as a preliminary method of habitat assessment, *Regulated Rivers-Research & Management*, *14*(5), 451-466.

Jung, H. C., and D. Alsdorf (2010), Repeat-pass multi-temporal interferometric SAR coherence variations with Amazon floodplain and lake habitats, *International Journal of Remote Sensing*, *31*(4), 881-901.

Jung, H. C., et al. (2010), Characterization of complex fluvial systems using remote sensing of spatial and temporal water level variations in the Amazon, Congo, and Brahmaputra Rivers, *Earth Surface Processes and Landforms*, *35*(3), 294-304.

Khan, S. I., et al. (2011), Satellite Remote Sensing and Hydrologic Modeling for Flood Inundation Mapping in Lake Victoria Basin: Implications for Hydrologic Prediction in Ungauged Basins, *Ieee Transactions on Geoscience and Remote Sensing*, *49*(1), 85-95.

Knighton, A. D. (1975), VARIATIONS IN AT-A-STATION HYDRAULIC GEOMETRY, *American Journal of Science*, *275*(2), 186-218.

Koblinsky, C. J., et al. (1993), MEASUREMENT OF RIVER LEVEL VARIATIONS WITH SATELLITE ALTIMETRY, *Water Resources Research*, *29*(6), 1839-1848.

Lee, H., et al. (2011), Characterization of terrestrial water dynamics in the Congo Basin using GRACE and satellite radar altimetry, *Remote Sens. Environ.*, *115*(12), 3530-3538.

Legleiter, C. J., et al. (2004), Passive optical remote sensing of river channel morphology and in-stream habitat: Physical basis and feasibility, *Remote Sens. Environ.*, *93*(4), 493-510.

Legleiter, C. J., and D. A. Roberts (2009), A forward image model for passive optical remote sensing of river bathymetry, *Remote Sens. Environ.*, *113*(5), 1025-1045.

Legleiter, C. J., et al. (2009), Spectrally based remote sensing of river bathymetry, *Earth Surface Processes and Landforms*, *34*(8), 1039-1059.

Leopold, L. B., and T. Maddock (1953), The Hydraulic Geometry of Stream Channels and Some Physiographic Implications, *Geological Survey Professional Paper*.

Lewis, L. A. (1966), ADJUSTMENT OF SOME HYDRAULIC VARIABLES AT DISCHARGES LESS THAN ONE CFS, *Professional Geographer*, *18*(4), 230-234.

Lu, Z., et al. (2005), C-band radar observes water level change in swamp forests, *Eos Trans. AGU*, *86*(14).

Marcus, W. A., and M. A. Fonstad (2008), Optical remote mapping of rivers at sub-meter resolutions and watershed extents, *Earth Surface Processes and Landforms*, *33*(1), 4-24.

Marcus, W. A., and M. A. Fonstad (2010), Remote sensing of rivers: the emergence of a subdiscipline in the river sciences, *Earth Surface Processes and Landforms*, *35*(15), 1867-1872.

Papa, F., et al. (2006), Wetland dynamics using a suite of satellite observations: A case study of application and evaluation for the Indian Subcontinent, *Geophys. Res. Lett.*, *33*(8), 4.

Park, C. C. (1977), WORLD-WIDE VARIATIONS IN HYDRAULIC GEOMETRY EXPONENTS OF STREAM CHANNELS - ANALYSIS AND SOME OBSERVATIONS, *Journal of Hydrology*, *33*(1-2), 133-146.

Prigent, C., et al. (2001), Remote sensing of global wetland dynamics with multiple satellite data sets, *Geophys. Res. Lett.*, *28*(24), 4631-4634.

Richards, K. S. (1973), HYDRAULIC GEOMETRY AND CHANNEL ROUGHNESS - NONLINEAR-SYSTEM, *American Journal of Science*, *273*(10), 877-896.

Richards, K. S. (1976), COMPLEX WIDTH-DISCHARGE RELATIONS IN NATURAL RIVER SECTIONS, *Geological Society of America Bulletin*, *87*(2), 199-206.

Shiklomanov, A. I., et al. (2002), Widespread Decline in Hydrological Monitoring Threatens Pan-Arctic Research, *EOS, Transactions, American Geophysical Union*, *83*(2), 13-20.

Smith, L. C., et al. (1995), ESTIMATION OF DISCHARGE FROM BRAIDED GLACIAL RIVERS USING ERS-1 SYNTHETIC-APERTURE RADAR - FIRST RESULTS, *Water Resources Research*, *31*(5), 1325-1329.

Smith, L. C., et al. (1996), Estimation of discharge from three braided rivers using synthetic aperture radar satellite imagery: Potential application to ungaged basins, *Water Resources Research*, *32*(7), 2021-2034.

Smith, L. C. (1997), Satellite remote sensing of river inundation area, stage, and discharge: A review, *Hydrol. Process.*, *11*(10), 1427-1439.

Smith, L. C., and T. M. Pavelsky (2008), Estimation of river discharge, propagation speed, and hydraulic geometry from space: Lena River, Siberia, *Water Resources Research*, *44*(3).

Stewardson, M. (2005), Hydraulic geometry of stream reaches, *Journal of Hydrology*, *306*(1-4), 97-111.

Stokstad, E. (1999), Hydrology - Scarcity of rain, stream gages threatens forecasts, *Science*, *285*(5431), 1199-1200.

Tetra Tech, I. (2005), FLO-2D Model Development Below Caballo Dam URGWOM Prepared For: U.S. Army Corps of Engineers.

U.S. Army Corps of Engineers (2004), Upper Mississippi River System Flow Frequency Study.

Vorosmarty, C. J., et al. (2010), Global threats to human water security and river biodiversity, *Nature*, *467*(7315), 555-561.

World Water Assessment Programme (2012), The United Nations World Water Development Report 4.